Multi-Parametric Analysis of Porous Radiant Burners

Marta Filipa Candelria Fidalgo
marta.fidalgo@ist.utl.pt

Instituto Superior Técnico, Lisboa, Portugal

October 2019

Abstract

Combustion within porous inert media is an effective way to obtain high radiant outputs for a large range of power densities, whilst simultaneously reducing pollutant emissions. It is well established that this phenomena is very complex in terms of the interaction between the different heat transfer modes, and the parameters that govern them hold much potential in terms of influence on the realm of performance optimization. Addition manufacturing allows for non-conventional porous media configurations to be manufactured, with endless possibility to tailor materials, geometric, thermal and radiative properties to a specific design demand. A series of multi-dimensional parametric investigations are conducted with the aim of characterizing the domain of optimal burner configurations, as it pertains to the radiant efficiency and the peak solid temperature. A one-dimensional model is employed, with two coupled energy equations for both gas and solid, multi-step chemical kinetics and the S_6 approximation to solve the RTE. The problem's parameters are de-coupled as much as possible, leaving aside existing property correlations. A study on the stability behavior of porous media combustion is carried out, aimed at better grasping the flame behavior, followed by the development of an driver code tasked with the autonomous management of 100k+ different inter-dependent burner case simulations simultaneously. It is found that, amongst the 8 parameters investigated, it is the emissivity, the excess air ratio, the extinction coefficient and the scattering albedo that are most determinant for achieving the best performance. The radiant efficiency is improved more than 50%.
Keywords: Combustion, Porous Media, Radiant Burner, Radiation, Multi-Parameter Analysis

1. Introduction

In light of diminishing reserves and increasing concerns about the consequences of large scale burning of fossil fuels on the planets' atmosphere and human life, interest in the development of alternative combustion technologies surged. Porous media combustion provides hope for cleaner and more sustainable combustion, with its trademark low emission rates, fuel interchangeability ability, which allows for the recycling of green-house gases like methane, and overall stable and flexible range of power densities. Also, the high burning rates, due to the preheating of the reactants made possible by the porous matrix, promise high radiant outputs.

Takeno *et al.* performed several studies [19, 20, 18] that introduced the idea of inserting a high thermal conductivity porous solid into the flame zone. Their analysis showed promise in the burning of low heat content fuels. Echigo *et al.* [2] was able to achieve a 60% reduction in fuel consumption by placing a permeable and optically thick solid in the reaction zone, when compared with a conventional burner with the same radiative output.

Hsu *et al.* [7, 6] furthered the modeling of PMC with introduction of multi-step kinetics and improved description of thermophysical properties. They identified the need for optimization of burner characteristics, operating conditions and geometry in order to influence performance goals like pollutant emissions or thermal efficiencies. Mital *et al.* [12] reported the first measurements of temperature and species distributions of the submerged reaction zone of a 2-layer porous radiant burners made of reticulated ceramic matrices and characterized them in terms of stability limits, radiant efficiencies and pollutant emissions. Reported radiant efficiencies were in the vicinity of 25%.

Diamantis *et al.* [1] developed a one-dimensional model, including full radiation and detailed chemistry, that captured both surface and submerged flames. The model employed fixed flame approach included radiation heat loss to the upstream environment. They studied flame profiles, burning velocities and radiant efficiencies for submerged flames. Peak radiant efficiencies achieved for submerged flames touched 25% for leaner mixtures.

Keramiotis *et al.* [11, 10] characterized porous burners with regards to thermal efficiency, pollu-

tant formation, operating limits. They also studied burner fuel interchangeability, performing experiments for both several different types of fuels. A range of thermal loads, equivalence ratios were studied, achieving stable combustion across the ranges. Radiant efficiency for 800 kW was around 25%. Hashemi [4] experimentally studied surface temperatures and radiant efficiencies of metal porous radiant burners for lengths. Maximum surface temperature is achieve for the thickest burner and radiant efficiency is maximum for the lower firing rate and higher thickness. Nejad and Nassab [14] investigated the effects optical thickness, scattering albedo, excess air ratio, and porosity on the radiant efficiency. Optical thickness was found to increase radiant efficiency by enhancing the absorption by the solid phase. Porosity, which was coupled to the porous matrix's surface area, had a negative effect on radiant efficiency. High excess air ratio and high scattering albedo also led to low radiant efficiency.

Horsman [5] performed the design optimization of the radiant efficiency of a 2-layer radiant burner through surface response modeling, with downstream pore size and porosity as design parameters. They obtained 30% improvement in the radiant efficiency and highlighted the importance of considering non-linear interactions between parameters. Randrianalisoa *et al.* [15] conducted investigations on the foam material for porous radiant burners. Their goal was to optimize energy efficiency and pollutant formation. They found that the optimal choice is lies in combination between different materials and porosity gradients.

The aim of this work is to investigate what is the set of characterizing porous burner parameters that maximize the radiant efficiency whilst keeping a solid temperature that preserves the burner's lifetime. A Progressive Parametric Study is carried out, in order to grasp the individual influence of each of the parameters on the radiant efficiency and the peak solid temperature, as well as their combined influence when studied in groups of 2 or all together. A 1D premixed flame model is employed to perform the required calculations, taking into account chemical kinetics, gas-solid temperature coupling and radiation modeling.

2. Modeling Background

2.1. Governing Equations

The problem considered is as follows: reactants enter the flame holder section, length L, and are preheated through convection by the solid matrix. The mixture ignites and energy is released by the flame. The gas-phase proceeds to convectively heat the solid matrix, which in turn conducts heat back upstream of the flame, whilst also radiating upstream and to the outlet environment. The premixed methane combustion is considered laminar, assuming one-dimensional geometry, negligible catalytic effects and isobaric flow. The porous solid is considered a isotropically difuse grey media and the gas phase is considered as non-participating media in radiation heat transfer. The governing equations become:

$$\text{Mass}: \quad \frac{\partial\left(\phi A \rho_g\right)}{\partial t}+\frac{\partial \dot{m}}{\partial x}=0 \tag{1}$$

$$\text{Gas}-\text{Phase Species}: \quad \phi A \rho_g \frac{\partial Y_k}{\partial t}+\dot{m} \frac{\partial Y_k}{\partial x}+\frac{\partial\left(\phi A \rho_g \nu_k Y_k\right)}{\partial x}-\phi A \dot{\omega}_k M W_k=0 \tag{2}$$

$$\begin{aligned}&\text{Gas}-\text{Phase Energy}: \\ &\phi A \rho_g C_{p,g} \frac{\partial T_g}{\partial t}+\dot{m} C_{p,g} \frac{\partial T_g}{\partial x}-\frac{\partial}{\partial x}\left(\phi A k_g \frac{\partial T_g}{\partial x}\right) \\ &+\phi A \sum_k\left(\rho_g C_{p,k} \nu_k Y_k\right) \frac{\partial T_g}{\partial x}+\phi A \sum_k\left(\dot{\omega}_k \bar{h}_k\right) \\ &+A H_v\left(T_g-T_s\right)=0\end{aligned} \tag{3}$$

$$\begin{aligned}&\text{Solid}-\text{Phase Energy}: \\ &(1-\phi) A \frac{\partial\left(\rho_s C_{p,s} T_s\right)}{\partial t}-\frac{\partial}{\partial x}\left(A k_{eff,s} \frac{\partial T_s}{\partial x}\right) \\ &+\frac{\partial(A Q_r)}{\partial x}-A H_v\left(T_g-T_s\right)=0\end{aligned} \tag{4}$$

where $\dot{m}=\phi A \rho_g S_L$ is the axial mass flow rate, cross-sectional area $A=1\ \mathrm{m}^2$ considered throughout. x denotes the axial coordinate and t the temporal one. Y_k refers to the mass fraction, ν_k the mass diffusion velocity, $\dot{\omega}_k$ the production rate and M_k the molecular weight of the k^{th} species. ρ_g denotes the gas mixture density. T_g and T_s the gas and solid phase temperatures, respectively, $C_{p,g}$, $C_{p,k}$ and $C_{p,s}$ the specific heat capacity for the gas mixture, species k and solid phase, respectively. The thermal conductivity of the gas mixture is denoted by k_g, and the effective thermal conductivity of the solid $k_{eff,s}$. $\bar{h_k}$ is the enthalpy of the k^{th} species, ρ_s the density of the solid, H_v the volumetric convective heat transfer coefficient and Q_r the radiative heat flux.

Boundary conditions

$$\text{Gas}-\text{Phase Species BCs}:$$

$$\text{inlet}: Y_k=Y_{k,in} \tag{5}$$

$$\text{outlet}: \frac{\partial Y_k}{\partial x}=0 \tag{6}$$

$$\text{Gas} - \text{Phase Energy BCs :}$$

$$\text{inlet} : T_g = T_{g,in} \tag{7}$$

$$\text{outlet} : (1-\phi)\, h_s \left(T_g - T_s\right) + \phi k_g \frac{\partial T_g}{\partial x}\Big|_- = 0 \tag{8}$$

$$\text{Solid} - \text{Phase Energy BCs :}$$

$$\text{inlet} : -k_s \frac{\partial T_s}{\partial x} - h_s \left(T_g - T_s\right) + \varepsilon\sigma\left(T_s^4 - T_{in}^4\right) = 0 \tag{9}$$

$$\text{outlet} : k_s \frac{\partial T_s}{\partial x} - h_s \left(T_g - T_s\right) + \varepsilon\sigma\left(T_s^4 - T_{out}^4\right) = 0 \tag{10}$$

where $h_s = H_v/S_v$ is the PIM surface convective heat transfer coefficient. With regards to the mass balance equation (1), no pre-determination of the value for $\dot{m}$ at the inlet or outlet is made. Instead, the flame location is prescribed by fixing the gas temperature at a point near the flame front region, as seen equation (11).

$$T_g \left(x = x_{flame}\right) = T_{flame} \tag{11}$$

Gas-phase related properties In order to get the density of the gas mixture the ideal gas equation of state is employed:

$$\rho_g = \frac{pMW_g}{RT_g} \tag{12}$$

The transport and thermodynamic properties of the gas mixture are calculated in function of temperature and mixture composition.

Chemical Kinetics The reaction rates necessary to compute the combustion heat release are given in the modified Arrhenius form:

$$k_f = AT^b \exp(-E/RT) \tag{13}$$

A 12-step augmented reduced mechanism [17] is used.

2.1.1 Porous Media properties

The effective thermal conductivity of the solid is computed with the parallel approximation (considering $k_s \gg k_g$) [9]:

$$k_{eff,s} = \phi k_g + (1-\phi)\, k_s \approx (1-\phi)\, k_s \tag{14}$$

where k_s is the bulk thermal condutivity of the material. The convective heat transfer is accounted by [16]:

$$\frac{H_v d_{pc}}{k_g S_v} = 0.3 + 0.664 Re^{1/2} Pr^{1/3} \tag{15}$$

Radiation Modeling The radiation term is calculated with the one-dimensional radiative heat transfer equations (RTE) [13]:

$$\mu \frac{\mathrm{d}I\left(\tau,\mu\right)}{\mathrm{d}\tau} + I\left(\tau,\mu\right) = \left(1-\omega\right) I_b\left(T_s\right) + \frac{\omega}{2}\int_{-1}^{1} I\left(\tau,\mu_i\right)\Phi\left(\mu,\mu_i\right)\mathrm{d}\mu_i \tag{16}$$

$$\frac{\mathrm{d}Q_r}{\mathrm{d}\tau} = \left(1-\omega\right)\left(4\pi I_b\left(T_s\right) - 2\pi\int_{-1}^{1} I\left(\tau,\mu\right)\mathrm{d}\mu\right) \tag{17}$$

with $\tau = \beta x$ as the optical depth. The corresponding boundary conditions are given by:

$$\tau = 0 \;:\quad I\left(\tau,\mu\right) = \varepsilon I_b\left(T_{in}\right) - \left(1-\varepsilon\right) 2\int_{-1}^{0} I\left(\tau,\mu_i\right)\mu_i \mathrm{d}\mu_i,\; 0 < \mu < 1 \tag{18}$$

$$\tau = \beta L \;:\quad I\left(\tau,\mu\right) = \varepsilon I_b\left(T_{out}\right) - \left(1-\varepsilon\right) 2\int_{0}^{1} I\left(\tau,\mu_i\right)\mu_i \mathrm{d}\mu_i,\; -1 < \mu < 0 \tag{19}$$

Both surfaces are considered here to be diffusely radiating grey surfaces, each facing an environment temperature of T_{in} and T_{out}, respectively. The inlet boundary is considered to be fully reflective.

The radiant efficiency is defined as the ratio between the radiant output and the thermal load of the combustion reaction:

$$\eta_{rad} = \frac{Q_{r,out} + (1-\phi)\,\varepsilon\sigma\left(T_{s,out}^4 - T_\infty^4\right)}{\phi\rho_g S_L Y_{CH_4} LHV_{CH_4}}, \tag{20}$$

with LHV_{CH_4} as the lower heating value for methane combustion.

2.2. Solution Method

The set of governing equations and corresponding sub-models presented are numerically solved with an adaptation of the PREMIX [8] code that incorporates the solid-phase energy equation, convective heat transfer between gas and solid phases, as well as the radiation model for which the S_6 approximation is used. The solution is obtained through a damped newton method that relies on an initial estimate for the gas and solid temperatures and species' distribution. Fixed flame position approach is taken with regards to the mass balance, but $\dot{m}$ is kept as a problem input by the use of an interface which iteratively changes the flame position in order to match the required mass flow rate.

3. Implementation

A multi-dimensional Progressive Parametric Study is carried out, which consists in three main stages: the first one is a 1D Parametric Study, where the

	1D & 2D		8D	
	Range	Points	Range	Points
$\boldsymbol{\phi}$	0.73 - 0.97	7	0.75 - 0.95	5
$\boldsymbol{S_v}$ [cm^{-1}]	2.0 - 23.0	7	5.0 - 20.0	5
$\boldsymbol{d_{pc}}$ [cm^{1}]	0.05 - 0.25	7	0.07 - 0.23	5
$\boldsymbol{\varepsilon}$	0.55 - 0.95	7	0.55 - 0.95	5
$\boldsymbol{\omega}$	0.3 - 0.9	7	0.3 - 0.9	5
$\boldsymbol{\beta}$ [cm^{-1}]	0.5 - 9.5	7	1.0 - 9.0	5
$\boldsymbol{k_s}$ [W/mK]	0.3 - 24.7	7	5.0 - 20.0	5
$\boldsymbol{\lambda}$	1.0 - 1.8	7	1.2 - 1.6	5

Table 1: Parametric domain for the different stages of the progressive parametric study.

influence of each individual variable is investigated. For the second stage the domain increases to 2D, in order to investigate the cross-influences between all parameter combinations. The last stage of the study consists on the extension of the analysis to the full discrete 8D Parametric Domain, on which the interest quantities are analyzed from different approaches. The goal is to understand which parameters are driving the interest quantities toward desirable values, how do the inter-parameter influences established affect them and to evaluate to which degree are the trends established on the first and second stage of the analysis can be assumed as general trends.

3.1. Design of Experiment

The ranges of each of the investigated parameters are presented in Table 1, along with the number of different values considered at every stage, which are uniformly distributed. The choice of bounds for each parameter is guided by the typical values present in the available literature but encompassing a larger range of variation, as much as possible. The parametric studies are performed for a range of combinations between three different input powers, 800, 1000 and 1200 kW, and three burner lengths, 1.0, 2.0 and 3.0 cm. The results presented here focus mainly on Q_{comb} = 1000 kW and L = 2.0 cm, unless stated otherwise. With regards to the interest quantities, the ceiling for maximum allowable solid temperature is set at 1750 K [3, 16]. With respect to the radiant efficiency it is this works' aim to achieve efficiencies higher than 25% [12, 1, 5].

3.2. Code Development

An application code of the numerical model, programmed in MATLAB in tandem with sh scripts is developed. The code uses a Systems of Decision approach in order to manage the large-scale computation of inter-dependent premixed combustion PRB cases, for 8 simultaneously varying parameters, and with the capability of dealing with non-linear convergence patterns, dynamic restart estimate assignment and effective case sequencing. The application code also included time management measures the curtail the time spent on failing simulations, which typically take much longer than converging ones.

On the whole, over 1 million different burner configurations/operating conditions were computed, for a total CPU time over 30000 hours. The simulations were ran on multiple machines at the same time, one with an AMD Ryzen 7 2700x eight-core processor with 1.8 GHz frequency and other three with Intel Xeon E5420 four-core processor, 2.5 GHz, both in hyper-threading, with the full set of runs taking two months to complete.

4. Results

The reference case for this study is Case 0 is presented in Table 2, which correspond to an input power of 1000 kW. The baseline radiant efficiency is 19.33% and the peak solid temperature 1738 K. The center cases are those that have the same set of properties as Case 0 but differ in Q_{comb} and L. The cases are also referred to as baseline for the studies characterized by the respective Power/Length combination.

4.1. One-Dimensional Study

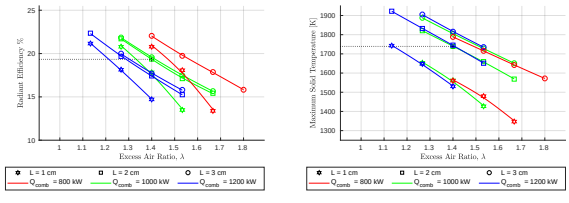

(a) (b)

Figure 1: Radiant efficiency and maximum solid temperature *versus* and excess air ratio, for different input powers and lengths: (a) η_{rad} *vs.* λ; (b) $T_{s,max}$ *vs.* λ.

ϕ	S_v	d_{pc}	ε	ω	β	k_s	λ	$\dot{m}$	L	$T_{g,in}$	T_∞
0.85	12.5	0.15	0.75	0.65	5	12.5	1.4	500	2.0	300	300
-	cm^{-1}	cm	-	-	cm^{-1}	W/m.K	-	g/s	cm	K	K

Table 2: Case 0 PIM characteristic parameters and operating conditions.

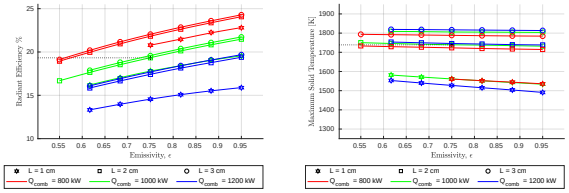

(a) (b)

Figure 2: Radiant efficiency and maximum solid temperature *versus* emissivity, for different input powers and lengths: (a) η_{rad} *vs.* ε; (b) $T_{s,max}$ *vs.* ε.

Fig. 1 shows the strong impact of the excess air ratio on η_{rad} and $T_{s,max}$. Lower excess air ratio (more fuel percentage) produces higher radiant efficiencies, along with an equally sharp increase in the maximum solid temperature. With increasing input power, the burner needs to increase the fuel percentage in order to achieve the same radiant efficiency, which also translates in an increase in maximum solid temperature. The PIM emissivity is positively correlated with the radiant efficiency and presents significant on this quantity (Fig. 2 (a)). Its influence on the maximum solid temperature is weak, but in the direction of improvement. The scattering albedo does not have a significant impact on η_{rad} except in its higher range, which penalizes strongly the radiant efficiency (Fig. 3 (a)). An increasing extinction coefficient produces decreasing radiant efficiency and increasing in maximum solid temperature, across all powers and lengths. The lower section of β presents a volatile behavior with strong non-linearities not easily categorized (Fig. 3 (b)).

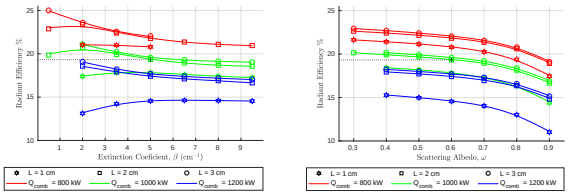

(a) (b)

Figure 3: Radiant efficiency *versus* extinction coefficient and scattering albedo, for different input powers and lengths: (a) η_{rad} *vs.* β (b) η_{rad} *vs.* ω.

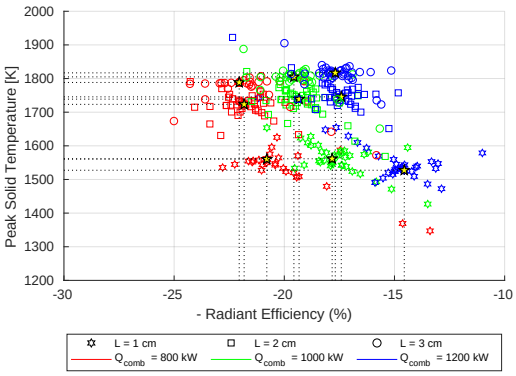

Figure 4: Cases computed for the 1D stage according to the input power and burner length.

Fig. 4 presents all of the computed 1D cases on the domain defined by $T_{s,max}$ *vs.* η_{rad} (Output Domain). It can be can be observed that the higher radiant efficiencies are achieved by the lowest input powers, consistent with what is reported in the literature [11, 10]. An increase burner length, on the other hand, leads to an increase in both radiant efficiency and peak solid temperature.

4.2. Two-Dimensional Study

An analysis of the parametric combinations for the reference Power/Length combination ($Q_{comb} =$ 1000 cm and $L = 2.0$ cm) is presented.

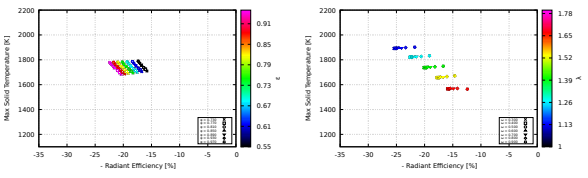

(a) (b)

Figure 5: Interest quantity domain for linearly independent parameters: (a) ϕ *vs.* ε; (b) ω *vs.* λ.

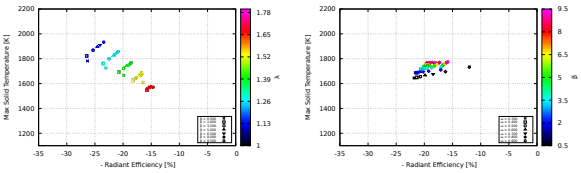

(a) Ouput domain of ω *vs.* k_s.

(b) Ouput domain of ω *vs.* β.

Figure 6: Image on the Output Domain of the variation of the extinction coefficient against the scattering albedo and excess air ratio.

The interactions between parameters can take one of two forms: linear combination, when the parameters are linearly independent, such as ϕ *vs.* ε and ω *vs.* λ (Figs. 5). In these cases, the shape of 1D curves for each parameter is repeated across variations. There are also distortion inducing interactions, which happen when one or both of the parameters introduce a change in the individual behavior of the other. Fig. 6 (a) illustrates the combined behavior of the extinction coefficient with the excess air ratio: a decrease in the excess air ratio (blue) increases the fitness of the lower values of the extinction coefficient (cross). The cross-influence can also be observed in the interaction between the scattering albedo and the extinction coefficient (Fig. 6 (b)): low values of extinction coefficient (black) increase the impact magnitude of the scattering albedo, an increase that emphasizes the negative effects of high ω (pentagon) on the radiant efficiency. With regards to β, it is also clear that the shape that describes the individual behavior of this parameter becomes distorted with changing ω: for lower values (cross) the curve becomes straighter in the low range of β (black), moving it toward a desirable zone of the Output Domain, whilst for higher ω (pentagon) the curvilinear shape at the bottom of β's range becomes more emphasized, increasing the penalty on η_{rad} and $T_{s,max}$.

Fig. 7 shows the scatter of all computed cases on the Output Domain, for both the 1D and 2D phases of the study across all the Power/Length combinations, along with the corresponding central cases. An increase of Q_{comb} is shown to produce an overall decrease in radiant efficiency across all burner lengths, whilst having little to no effect on the peak solid temperature. An increase in burner length, on the other hand, influences positively η_{rad}, albeit not significantly. The effect on $T_{s,max}$ is more significant, producing a temperature increase of around 250 K, with increasing L for the center (baseline) cases and an increase in incidence of cases above the maximum allowable temperature (1750 K), especially for $L = 3.0$ cm. This is likely caused by the increase in surfaces available for convective heat transfer from the gas, allowing more energy to be transferred to the solid, without there being a matching outlet mechanism for this energy. This analysis is observable for the bulk of the cases' swarm for each Power/Length combination, despite there being some outliers with more irregular behavior. On the whole, the most desirable PL pair for the purposes of this work is the case with $Q_{comb} = 800$ kW and $L = 2.0$ cm, with high radiant efficiencies and peak solid temperatures below the limit.

4.3. Full Eigth-Dimensional Study

A total of 1012793 different cases were computed in this stage, for 3 different burner lengths and 2 different input powers. Figure 8 illustrates the placement of the four sets of 8D studies on the Output Domain, along with the ones from the previous stages of the Progressive Parametric Study.

A larger range within the Output Domain is achieved, when compared to the previous stage, both toward desirable and undesirable results of both interest quantities, as would be expected. For all sets of cases an increase of at least 10% in η_{rad} ($\sim$ 50% relative improvement) is achieved when compared to the respective center case.

Overall, the behavior of the input power and burner length defined in the previous stages is confirmed.

The set with $L = 3.0$ cm presents similar radiant efficiencies to the reference case set , however more than half the cases are above the temperature limit for the solid (1750 K). The set with $L = 1.0$ cm confirms the tendency established in the 2D parametric study for this burner length, where the parametric interactions tend to emphasize poorer radiant efficiencies, with a large portion of the cases in the 8D study falling to the lower side of η_{rad}. It presents good peak temperature values in its highest η_{rad} zone, but falls short in the radiant efficiency when compared to its counterparts.

The case with $Q_{comb} = 800$ kW is the one that reaches higher radiant efficiencies than all other PL combinations (as expected [10, 11]), all well within the required temperature limits, once more sustaining that this is the most desirable Power/Length combination for the purposes of this work.

It is also relevant to note that the Pareto front is linear and has similar a slope for all sets of studies in Fig. 8. The points at the possibility of a relationship between the peak solid temperature and and the radiant efficiency (equivalente to radiant output in this case) that defines the ceiling of these two quantities from an optimization standpoint.

Parameter Scatter Visualization Presents a visualization of the index distribution of each parameter, with the aim of providing a visual under-

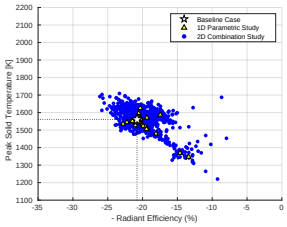

(a) Q_{comb} = 800 W and L = 1.0 cm.

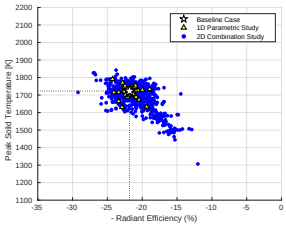

(b) Q_{comb} = 800 kW and L = 2.0 cm.

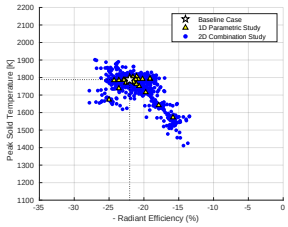

(c) Q_{comb} = 800 kW and L = 3.0 cm.

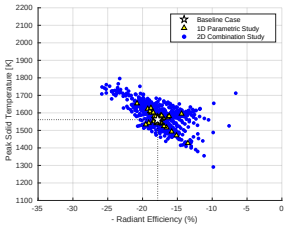

(d) Q_{comb} = 1000 kW and L = 1.0 cm.

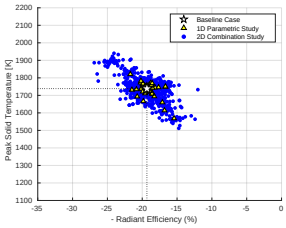

(e) Q_{comb} = 1000 kW and L = 2.0 cm.

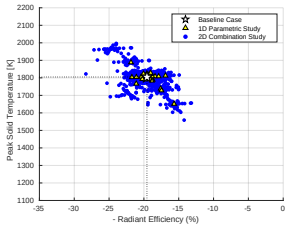

(f) Q_{comb} = 1000 kW and L = 3.0 cm.

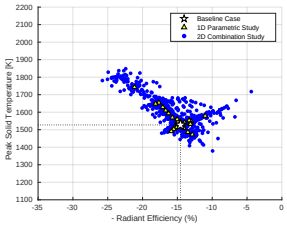

(g) Q_{comb} = 1200 kW and L = 1.0 cm.

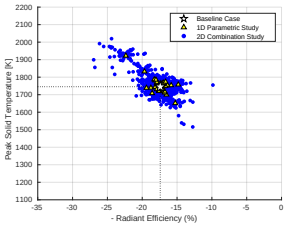

(h) Q_{comb} = 1200 kW and L = 2.0 cm.

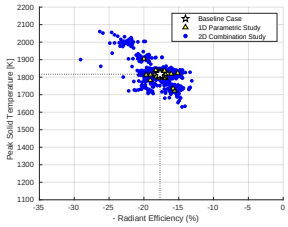

(i) Q_{comb} = 1200 kW and L = 3.0 cm.

Figure 7: Output Image of the cases computed for the 1D and 2D Parametric Study, for all input powers and burner lengths.

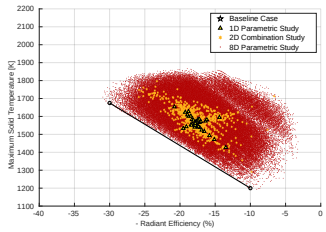

(a) Q_{comb} = 1000 kW and L = 1 cm.

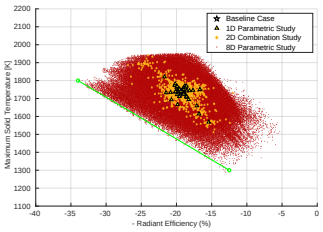

(b) Q_{comb} = 1000 kW and L = 2 cm.

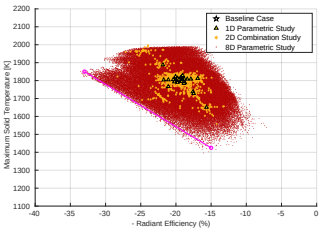

(c) Q_{comb} = 1000 kW and L = 3 cm.

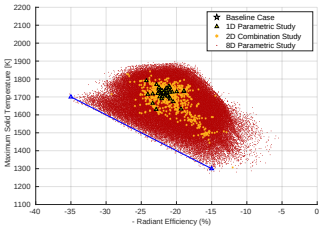

(d) Q_{comb} = 800 kW and L = 2 cm.

Figure 8: Scatter map of the distinct phases of the Progressive Parametric Study for 4 different Power/Length combinations, including the respective center/baseline cases and Pareto fronts.

standing of how the problem's parameters relate to the position of each case in the interest quantity domain.

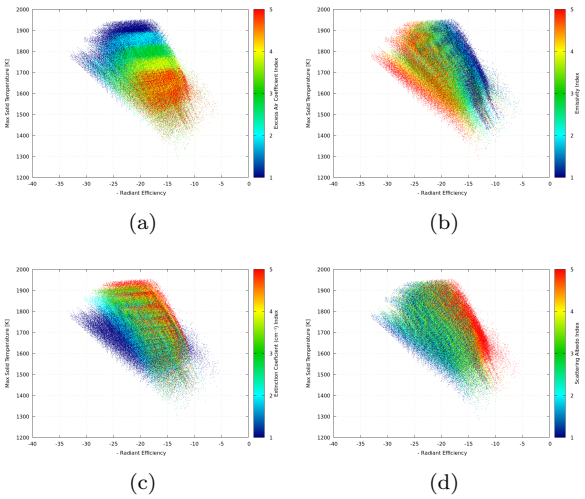

Figure 9: Examples of parametric distributions on the Output Domain: (a) Excess Air Ratio; (b) Emissivity ; (c) Extinction Coefficient; (d) Scattering Albedo.

Fig. 9 (a) and (b) shows that the excess air ratio and the emissivity present clearly defined behavior with regards to the interest quantities. The index distribution is well sorted, showing that this parameter is strongly correlated to the performance parameters of a porous burner. The distributions mimic the behaviors established in the 1D study. The extinction coefficient presents an interesting distribution (Fig. 9 (c)), with the Pareto front being clearly dictated by $\beta = 1.0$ cm^{-1}. This value of the extinction coefficient is also responsible, however, for some of the worst performing cases, a statement to the extinction coefficient's ability to either improve or worsen the overall performance of the burner depending on its conjugation with other parameters. This conjugation effect is most clearly observed in the combination with ω (Fig. 9 (d)) where these points with low β correspond to points with higher scattering albedo ($\omega = 0.9$), echoing the 2D parameter from these parameters.

Desirable zones The analysis is centered on the Desirable and the Most Desirable zones of the Output Domain, that are located on the Pareto front of the parametric distribution. The most Desirable zone is defined as the set of cases that have a radiant efficiency above 25%, the maximum achieved in previous stages of the study. The ceiling for the maximum solid temperature is set at 1750K. The Most Desirable zone is an approximation made to the "optimal point" with regards to radiant efficiency and solid maximum temperature. It is defined as a rectangle (1% by 10 K) that lies on the Pareto front, at the zone with the highest radiant efficiency that is below the temperature ceiling. Fig. 10 shows the full domain, the Desirable zone and the Most Desirable zone.

A statistical analysis is performed on the Desirable and Most Desirable in order to carve out what are the parameters are actually determinant for the performance purposes of this work. The probability distribution function for the parameters in these zones yield the results in Fig. 11. The extinction coefficient is the most polarized parameter, with a clear preference for the lower values in the Desirable zone and a 100% incidence of $\beta = 1.0$ cm^{-1} on the Most Desirable zone for both input powers. The emissivity has a strong preference for the higher values in the Desirable zone, strongly emphasized in the Most Desirable zone. The excess air is more frequently found near lower values, in a less severe way than β and ε. The scattering albedo is more successful for its lower values in both zones, with $\omega = 0.9$ being the undesirable one.

Note that the preference for low β and high λ, as well as the need to avoid ω is in complete concordance with the findings in the 2D parametric study. Indeed it is these 3 parameters, along with ε that are the ones that drive the radiant performance and temperature of a porous radiant burner.

The right-hand side of Fig. 11 also features a description of the case fitness for the parameters in the Desirable zone. Large bubbles near the x axis mean that the Index in question is very prevalent near the Most Desirable zone. This strengthens the results of the PDFs, while simultaneously increasing the robustness of the results.

All the parameters exhibit flexibility in the parameter predictions except for the extinction coefficient which proves to be a very important parameter.

5. Conclusions

The Progressive Parametric Study confirms the importance of the most influential parameters throughout all three stages. The excess air ratio and the emissivity have a high impact, which is maintained when other parameters are introduced in the analysis. The excess air ratio produces an enhancing effect on the impact of lower extinction coefficient values, mimicked in the full 8D parametric analysis. The extinction coefficient presents a weak impact on the interest quantities in the 1D analysis, but is prone to introduce cross-influences when combined with other parameters. One example is the combination with the scattering albedo, combination that both can lead to improvement or significant penalty on the radiant efficiency and peak solid temperature. Overall, excess air ratio, emissivity, extinction coefficient and scattering albedo

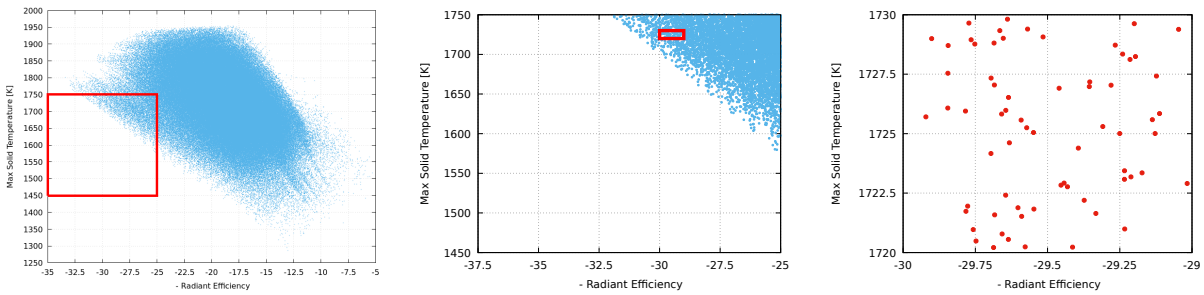

(a) (b) (c)

Figure 10: Illustration of the Desirable and the Most Desirable zones for the two input powers: (a) - (c) $Q_{comb} = 800$ kW ; (c) and (d) - (e) $Q_{comb} = 1000$ kW.

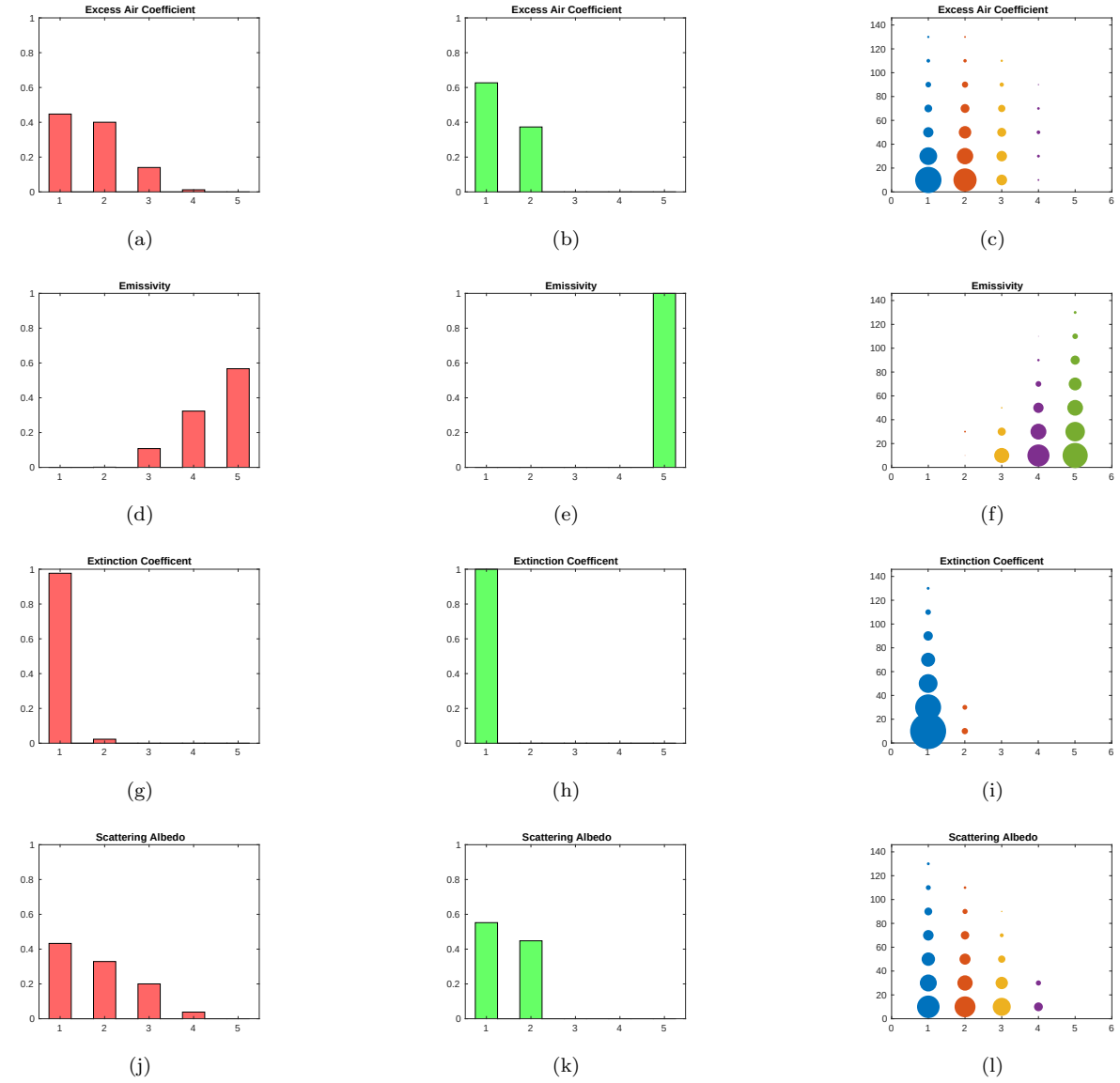

(a) (b) (c)

(d) (e) (f)

(g) (h) (i)

(j) (k) (l)

Figure 11: Probability Distribution Function (PDF) for the problem's parameters, in the Desirable and Most Desirable zones, respectively, for $Q_{comb} = 1000$ kW: (a) and (b) Porosity; (c) and (d) Specific Surface Area; (e) and (f) Characteristic Pore Diameter; (g) and (h) Emissivity; (i) and (j) Scattering Albedo; (k) and (l) Extinction Coefficient; (m) and (n) Solid Thermal Conductivity; (o) and (p) Excess Air Ratio.

are the parameters that are fundamental in order to achieve improvements in the PRB radiant performance. For the reference Power/Length combination an improvement of 50% in the radiant efficiency was obtained, for maximum solid temperatures below 1750 K. It was also found that these trends do not change significantly with the power density of the burner, in opposition to the flameholder length, which induces changes in the variables impact for shorter lengths.

References

[1] E. M. D.J. Diamantis and D. Goussis. Simulations of premixed combustion in porous media. *Combustion Theory and Modelling*, 6(3):383–411, 2002.

[2] R. Echigo, K. Ichimiya, M. Kurusu, and Y. Yoshizawa. Combustion augmentation of extremely low calorific gases: application of the effective energy conversion method from gas enthalpy to thermal radiation. In *Proceedings of the ASME JSME Thermal Engineering Joint Conference, Honululu*, volume 4, pages 99–104, 1983.

[3] GoGaS Goch GmbH and Co. KG, Zum Ihnedieck 18, 44265 Dortmund, Germany. *M High Intensity Heater*.

[4] S. A. Hashemi, M. Nikfar, and R. Motaghedifard. Experimental study of operating range and radiantion efficiency of a metal porous burner. *Thermal Science*, 19(1):11–20, 2015.

[5] A. Horsman and K. Daun. Design optimization of a two-stage porous radiant burner through response surface modeling. *Numerical Heat Transfer; Part A: Applications*, 60(9):727–745, 2011.

[6] P.-F. Hsu, W. D. Evans, and J. R. Howell. Experimental and numerical study of premixed combustion within nonhomogeneous porous ceramics. *Combustion Science and Technology*, 90(1-4):149–172, 1993.

[7] P.-F. Hsu, J. Howell, and R. Matthews. A numerical investigation of premixed combustion within porous inert media. *Journal of Heat Transfer - Transactions of the Asme*, 115:744–750, 08 1993.

[8] R. J Kee, J. F Grcar, M. D Smooke, J. A Miller, and E. Meeks. *PREMIX: a fortran program for modeling steady laminar one-dimensional premixed flames*. Sandia National Laboratories, 01 1985.

[9] M. Kaviany. *Principles of heat transfer in porous media / M. Kaviany*. Springer-Verlag New York, 1991.

[10] C. Keramiotis, M. Katoufa, G. Vourliotakis, A. Hatziapostolou, and M. Founti. Experimental investigation of a radiant porous burner performance with simulated natural gas, biogas and synthesis gas fuel blends. *Fuel*, 158:835 – 842, 2015.

[11] C. Keramiotis, B. Stelzner, D. Trimis, and M. Founti. Porous burners for low emission combustion: An experimental investigation. *Energy*, 45(1):213 – 219, 2012.

[12] R. Mital, J. Gore, and R. Viskanta. A study of the structure of submerged reaction zone in porous ceramic radiant burners. *Combustion and Flame*, 111(3):175 – 184, 1997.

[13] M. F. Modest. *Radiative Heat Transfer*. Academic Press, Boston, third edition, 2013.

[14] H. S. Nejad, S. A. G. Nassab, and E. J. Javaran. Numerical study on radiant efficiency of a porous burner under different conditions. *Journal of Thermophysics and Heat Transfer*, 32(2):475–482, 2018.

[15] J. Randrianalisoa, Y. Brchet, and D. Baillis. Materials selection for optimal design of a porous radiant burner for environmentally driven requirements. *Advanced Engineering Materials*, 11(12):1049–1056, 2009.

[16] M. Scheffler and P. Colombo. *Cellular Ceramics: Structure, Manufacturing, Properties and Applications*. Weinheim: Wiley-VCH, 2005.

[17] C. Sung, C. Law, and J.-Y. Chen. An augmented reduced mechanism for methane oxidation with comprehensive global parametric validation. *Twenty-Seventh Symposium (International) on Combustion*, 27(1):295 – 304, 1998.

[18] T. Takeno and K. Hase. Effects of solid length and heat loss on an excess enthalpy flame. *Combustion Science and Technology*, 31(3-4):207–215, 1983.

[19] T. Takeno and K. Sato. An excess enthalpy flame theory. *Combustion Science and Technology*, 20(1-2):73–84, 1979.

[20] T. Takeno, K. Sato, and K. Hase. A theoretical study on an excess enthalpy flame. *Eighteenth Symposium (International) on Combustion*, 18(1):465 – 472, 1981.